An Integrated Study of Gravity and Magnetic Data to Determine Subsurface Structure and Depth to Basement in Alamein Area, Western Desert, Egypt.

Ismail S. Ismail[1], Saada A. Saada[1], Youssef M.Y. Ali[2] and Youssef M.Y. Ibrahem[2].

[1]*Geology Department, Faculty of Science, Suez University, Suez, Egypt.*
[2]*Science and Math Engineering Department, Faculty of Petroleum and Mining Engineering, Suez University, Suez, Egypt.*

Abstract:*The present study wascarried out to delineate the location, extension, trend and depth of subsurface structures of Alamein area. To achieve this aim, the gravity and aeromagnetic data have been subjected to different analytical techniques. The Fast Fourier Transform technique was used to separatethe residual components from the regional ones. The resulted maps showed that the area was affected mainly bytheENE, E-W, WNWand NWtectonic trends. In addition, spectral analysis technique was applied on magnetic anomalies to estimate the depth to basement surface, which varies from 3.03 in southern part to 7.24 Km in northern part.3D-Eulerdeconvloution and tilt angle derivative techniques were carried out to detect the edges of magnetic sources and to determine their depths.Correlation between them shows acoincidence between Euler solution and zero lines of tilt angle map. A tentative basement structure map is constructed from the integration of these results and geological information. This map shows alternative uplifted and downfaulted structure trending in the ENE, NE and E-W directions. In addition, the NNW to NW strike-slip faults intersected them in later events. Finally, 2-D modeling technique was run on three gravity and magnetic profiles in the same location. Different drilled wells and the constructed basement structure map support these modeled profiles. Theyshow an acidic basement rocks. A general decreasing of Conrad discontinuity depths from about 20.5 km at southern part to 17.9 km at northern part can be noticed. Moreover, the crustal thickness (depth to Moho discontinuity), varies between 31.5 and 28.5 km revealing visibly crustal stretching and thinning northerly.*
Keywords: Basement, Euler's deconvolution, Fast Fourier, Modeling, Tilt angle derivative.

I. Introduction

The Western Desert covers a surface area of about 700.000 km[2]. The study area lies in the northern portion of the Western Desert between Latitudes 30°, 00' and 31°, 00', N and Longitudes 28°, 00' and 29°, 00' E. It lies on the northern margin of the Western Desert and extends from the shoreline's zone adjacent to the northeastern margin of Qattara Depression. It covers a surface area of about 10450 km[2] (Fig.1).

The area is characterized by complex structures developed due to interaction of different tectonic events. As the study area is a part of northern Western Desert, so many authors constructed structure maps to delineate the subsurface basement structure. [1] illustrated the presence of basement mega structure in Western Desert, where the study area comprises two structure namely, Dabaa high and Sharib-Sheiba high, in northern and southern part respectively, while Gibb-Afia high extends from SiwaOasis to northwestern edges of Qattara Depression. Meanwhile, [2] constructed more reliable basement tectonic map (Fig.2). It shows three subsurface structure only in the investigated area; Gibb-Afia high that is trending in the NE direction at the middle part; Ras-Qattara uplifted, which is trending in the E-W at southern part and Alamein basin lies between them.

[3] analyzed Apatite fission track data from recent wells that were drilled to basement rocks. It indicated that the Sheiba High basement blocks, with the NE direction, formed during the Early Jurassic, and were not significantly affected by subsequent tectonic events. However, recent studies based upon regional 3D and 2D seismic interpretation and well data suggest that the Jurassic rifts have more of an east-west orientation [3]

However, the gravity field gives an integrated response to density contrasts caused by structural features on regional and local scales. While structural features occur above the Curie isotherms of magnetic crustal rock minerals may yield contrasts in magnetic attributes making them visible on magnetic maps [4].Therefore, the present study was carried out using integrated approach of processing and interpretation of both Bouguer gravity and aeromagnetic data, as well as available geological data to construct more reliable structure basement map depending on the interpretation of recent analytical method. In addition, coupling between 2-D gravity and 2.5-D magnetic modeling follows scientific step to minimizing errors and build magnetic portion according to structure element from basement map. Finally, the output of gravity and magnetic

modeling, results will be integrated in order to evaluate subsurface structure, crustal continental type and to map the basement surface.
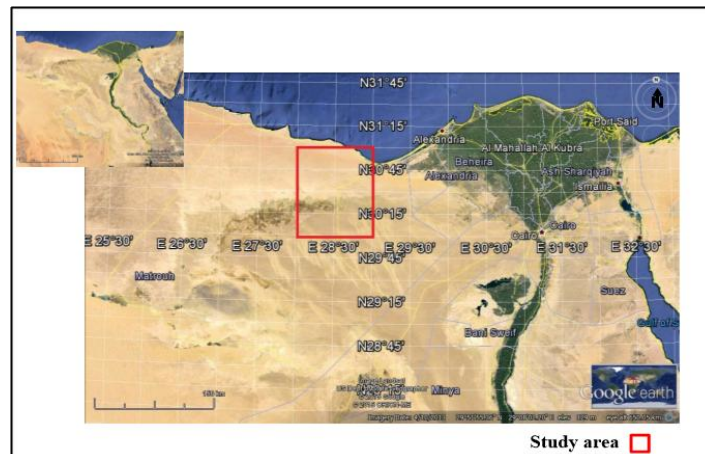

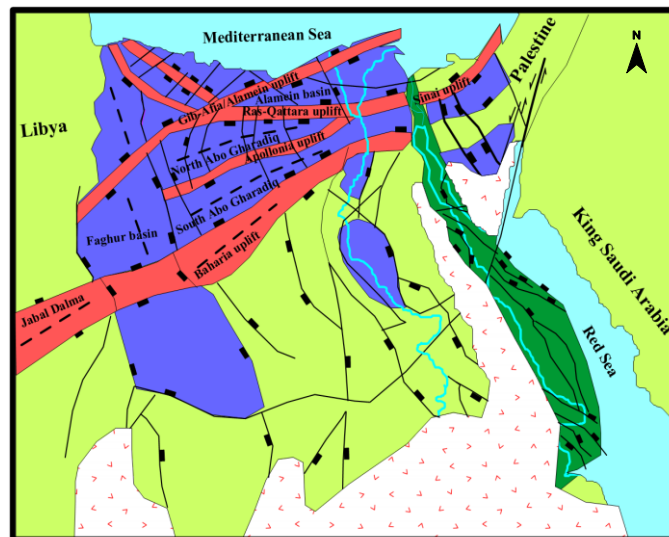Fig.1: Location map of the study area.

Fig.2: Basement tectonic map of the Western Desert of Egypt (After [2]).

II. Geological Setting

Geomorphologically, the outcrops of the investigated area are shown as Sand and Clay-rich units of Early Miocene at the northeastern part of the Qattara Depression, while Calcareous Sands and Clay-rich sediments of Middle and Late Eocene and Oligocene ages lie in the southern and western boundaries of the depression. The area in and around Moghra Lake is mostly covered by Quaternary deposits. Unconsolidated eolian Sands, Sabkha deposits, and wadi fill unconformably overlying the Miocene rocks represent the Quaternary deposits [5].

The generalized stratigraphic column of the northern Western Desert (Fig.3), where the studied area is located, shows that the subsurface stratigraphic sequence is ranging in age from Cambro-Ordovician to Recent, resting unconformably over the crystalline basement rocks [6]. [7] subdivided the whole sedimentary section of the northern Western Desert into the lower clastic division (Cambrian to Early Mesozoic), the middle calcareous division (Cenomanian to Late Eocene), and the upper clastic division (Oligocene to Recent).

III. Tectonic Setting

Tectonically, the northern Western Desert represents a part of the unstable belt of the tectonic framework of the Egyptian Territory ([8], [9] and [10]). The investigated area has been subjected to different tectonic regimes since the Precambrian time to Recent. Precambrian exhibit three tectonic trends namely, Nubia (N-S), Red sea (NNW) and Tibesti (NE) trends, which are inherited in basement rocks of the northern Western Desert ([11] and [2]).

New tectonic trend appeared in Paleozoic time resulted from thrusting or uplifting of Africa continent against the main block of the earth`s crust might have been cause of the formation of E-W trend. This trend is shown in the Gulf of Suez and northern Western Desert in Regional magnetic and isopach maps [11]. In addition, strong E-W tectonic trend is shown in many parts of isopach maps of successive formation (e.g. Masajid and Khattatba formation) of middle-upper Jurassic which indicating that the deposition of sediments from Late Paleozoic to Late Jurassic was controlled by E-W tectonic trends [11].
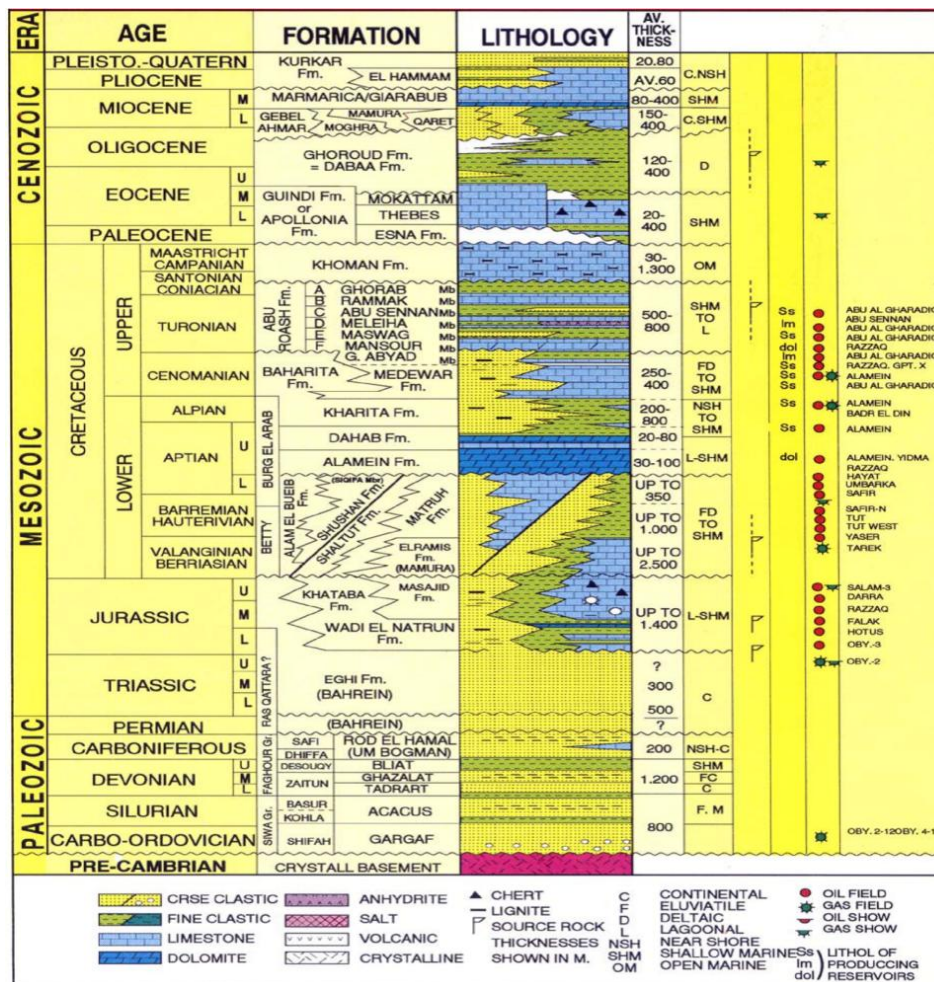

Fig.3: Generalized Stratigraphic Column of Western Desert (after [12]).

New events appear in Late Jurassic to Early Tertiary resulted from movements of Africa relative to Lurasia (Tethyan plate movement). These activity appear in two phases ([1], [11] and [13]); (1) The Sinsitral shear movements during Late Jurassic to Early Cretaceous (Nevadian event), so two tectonic elements recorded with wrench master E-W faults, NW fold which associated thrust faults and ENE strike slip faults[14]. (2) The Dextral shear movements during Late Cretaceous to Early Tertiary (Laramide event), so two tectonic elements recorded with wrench master E-W faults, ENE fold (Syrian arc system) trend which associated thrust faults and WNW strike slip faults.

After dextral lateral movements in Late Cretaceous to Early Tertiary followed by northward motion of Africa toward Laurasia produced the Alpine orogeny ([15] and [16]), where two resulted compressive forces N-S and NNW-SSE trend. [17] suggested 20° shifted in northern compressive forces and add that these NNW compressive forces resulted in ENE trend Uplifted and thrust in northern Egypt from Early Tertiary to Middle Eocene. Middle Tertiary appear a new regional extensional forces ENE-WSW resulted two complementary primary shear rifting system NW-SE (Red sea or Gulf of Suez trend) and NNE-SSW (Aqaba trend)[11].

IV. Available data

The available data include:

---

1. The Bouguer anomaly map, compiled by the General Petroleum Company [18] with a scale of 1:100,000 and contour interval of 1 mGal.
2. The total intensity aeromagnetic map, compiled by Gulf of Suez Petroleum Company [19] with a scale of 1:250,000 and contour interval of 10 nT.
3. The available geologic data consist of 34 wells reached to different formations (Table.1).

Table.1: Information derived from drilled wells in the study area.

Well no.	Symbol	T.D.(km)	FMTD	Status
MAS-1X	1	3	AEB#3	Succ. Well (Oil)
N. ALAMEIN-1X	2	3.55	AEB # 3E	OIL PRODUCER FROM ALAMEIN
ALAMEIN-1	3	4.4	L. CRETACEOUS	OIL PRODUCER L. Cretaceous
BEA-4	4	2.63	L. BAHARIYA	REC. OIL
HORUS-1	5	2.73	APTIAN	OIL PRODUCER U. Cretaceous
HORUS-2	6	2	BAHARIYA	OIL PRODUCER U. Cretaceous
HORUS-3	7	2	CENOMANIAN	OIL PRODUCER U. Cretaceous
YIDMA-1	8	2.74	L. CRETACEOUS	OIL PRODUCER L. Cretaceous
RAZZAK-15	9	2.68	L. APTIAN	OIL PRODUCER U. Cretaceous
N. RAZZAK-2	10	2.6	AEB	Succ. Well (Oil)
RAZZAK-1	11	3.37	JURASSIC	OIL PRODUCER U&L. Cretaceous
AGHAR-2X	12	1.9	BAHARIYA	OIL PRODUCER U. Cretaceous
QATTARA RIM-2X	13	2.37	ALAM EL BUEIB MBR	OIL PRODUCER
S. DABAA 9-2"st"	14	3.87	BAHREIN	Succ. Well
TOPAZ-1X	15	3	AEB #3A	P & A
RETHEM-1	16	2.8	APTIAN	P & A
DAHAB-3X	17	3.6	AEB	P & A
N.R.Qattara-4x	18	2.4	BAHARIYA	P & A
DABAA-3X	19	3.2	ALAM EL BUEIB MBR	P & A
SANHUR-1	20	2.8	L. CRETACEOUS	P & A
DABAA-2X	21	4.5	KHATTATBA	P & A
N.YIDMA-1	22	3.1	APTIAN	P & A
ALMAZ-1	23	4.1	Basement	P & A
S. DABAA 8-1, ST	24	2.9	Basement	P & A
Ig 34-1	25	4.6	MASAJID	P & A
HORUS-7	26	3.32	AEB	P & A
RAZZAK-18	27	2.58	AEB	P & A
JG-A	28	3.34	BAHREIN	P & A
FADDA-1	29	4.8	KHATATBA	P & A
GANAYEN-2	30	4.86	KHATATBA	P & A
OBEID ALLAH-1	31	3.9	JURRASIC	P & A
EL KLISH-1	32	2.8	MASAJID	P & A
SHEIBA-1	33	2.5	PALEOZOIC	P & A
JG-B "st"	34	3.45	BAHREIN	P & A

V. Methodology and results

5.1. Bouguer map description

The Bouguer anomaly map of the study area (Fig.4), exhibits that the amplitude ranges from (-7) mGals to (+25) mGals. Positive anomalies exist at the northern and southern parts of the study area with sharp anomalies. At these parts, the high values of gravity anomalies may be associated with the basement, uplifts and/or horsts. Closed and subclosed anomalies at southern part of the study area (West to Moghra lakes), include the maximum positive anomaly (24 mGals), with main NE to ENE trends.Linear anomalies may be associated with fault of the basement rocks and/or the sedimentary cover trending mainly E-W direction north to Well no. 29 and around well no. 32, while trending NE around well no. 14. Appearance of linear patterns and prominent steep gradients on previous locations may be suggest existence of major basement fault lines [20]. Closed negative anomalies, may be related to sedimentary basin and/or grabens. The interested area has two main low negative anomalies; Western anomaly lies around well no. 30 and trending mainly in the NE direction, while, eastern one includes most of product wells, with E-W trend.

5.2. Magnetic data processing and description

The total aeromagnetic data of the study is used to construct the Reduced to Pole (RTP) map. The average magnetic inclination is 43.7° N and declination is 1.8° E. The RTP aeromagnetic map was deduced by subtracting the theoretical main field, which calculated by IGRF (International Geomagnetic Reference Field) using [21].In addition the zero level is the reading at the points where there is no appreciable disturbance from subsurface masses; so that, only the normal magnetic field is present [22]. The constructed RTP, relative to zero level, map (Fig.5) becomes the starting map on both qualitative and quantitative interpretation.

RTP aeromagnetic map, relative to zero level (Fig.5) represented mainly by negative anomaly in northern part and positive anomalies in southern parts. The negative anomaly (around well no. 3, 29 and 30) is

the largest and the simplest one. It has the minimum value of about -40 nT. This anomaly appeared as closed, broad, and gentle slope that may be associated to basin, grabben or variation in mineralogical composition, with ENE direction. Furthermore, linear anomalies with high gradient (north to well no. 29) could be associated with faults are running mainly in, E-W and NE directions. In addition, the middle part of magnetic map exhibits a linear pattern in NE to ENE and E-W directions. The southern part (West to Moghra lakes) shows a group of closed or subclosed positive anomalies characterized by wide range of magnetic values from 180 to 340 nT oflow, moderate and high amplitudes. These anomalies appear with the same location in Bouguer map, which may be associated to Ras-Qattara high.
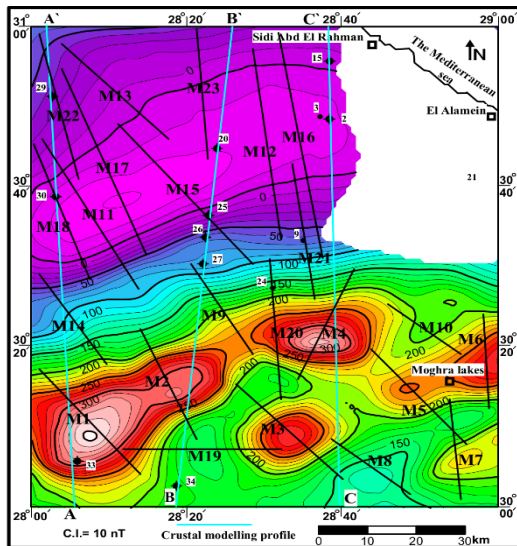

Fig.5: RTP aeromagnetic map of the study area, relative to zero level showing the location of crustal modelling profiles and spectral analysis profiles used in depth estimation.
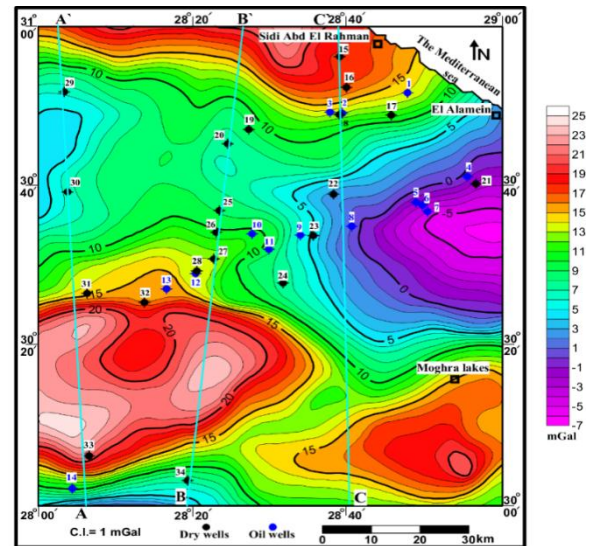

Fig.4:Bouguer anomaly map of the study area. (After [18]) showing the location of crustal modelling profiles.

5.3. Regional-Residual separation

The potential anomaly measured at the surface is not produced by one simple structure, but it is the sum of the effects of a number of subsurface structures buried at various depths. First step to construct crustal modeling begins by isolation of the regional constituents away from the local ones. In present study, Fast Fourier Transform (FFT) technique is applied on both Bouguer and RTP maps to separate shallow structure (High-pass) from deep seated ones (Low-pass).In addition, Band-pass filtering is applied to detect true anomalies resulted after cutting deep seated and shallow noise effects.

The process began by converted gridded data from space domain into frequency domain using [21], where averaging all direction for the same wavenumber to product 2-D Radial average power spectrum curves. The most advantage of this method, it is depended on selective wavenumber from 2-D power spectrum curves. In other words, it is related to experience and knowledge of interpreter to estimate best fit for deep, intermediate and shallow zones, where a point intersection between these fitted lines become our selective point to separate by using wavenumber values. The energy power spectra are shown in (Figs.6 and 7) for both gravity and RTP data of the studied area.
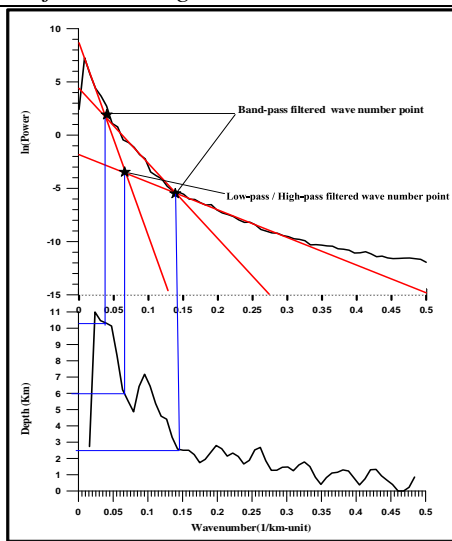
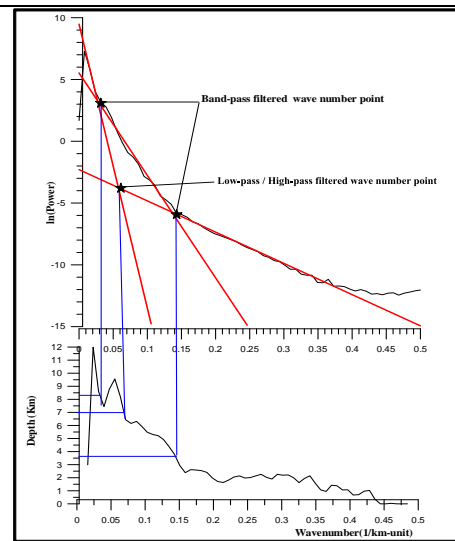Fig. 6: 2-D power spectrum Bouguer map.   Fig.7: 2-D power spectrum RTP (zero level) map.

The low-pass (regional) gravity filtered map (Fig.8) reveals the wavenumber lesser than 0.0145 cycle/km. This map comprises a group of strong anomalies of different shapes, orientations, and extensions, which show the regional anomalies, related to deeper sources. These anomalies are described as broad and high wavenumber as shown by decreasing the sharpness with the same trend patterns exist in Bouguer map (Fig.4). While, High-pass filtered gravity map (Fig.9) resulted from cut-off wavenumber longer than 0.0145 cycle/km, which appears as local fluctuations of small closures and noses in the contours, trending mainly in the E-W and ENE directions.

Band-pass gravity filtered map (Fig.10) is isolated by pass wavenumber between 0.0277- 0.0073 cycle/km. Generally, this map gives a good idea about the distribution of the depressions and ridges with their extension in the area as compared with the high-pass map (Fig.9).The map shows low regional gravity anomalies in the middle part split into a large number of small residuals. It reveals new negative anomalies that could be interpreted as new basins, and exhibits other positive ones that considered as promising sites of hydrocarbon. These anomalies are trending mainly in the E-W, ENE to NE, WNW, and NW directions. This map shows good observation to zero lines, which may be outline major faults in similar high gradient parts described before in Bouguer map as shown in northern (north well no. 29), middle (south well no. 32 and close to well no. 9) and southern (around well no. 14) parts.

Low-pass filtered magnetic map (Fig.11) is constructed by passing wavenumber longer than 0.0173 cycle/km. This map includes similar shapes and trends similar to the original map but with lesser magnitude and more smoother. Furthermore, Figure (12) displays the high-pass filtered map made by removing wavenumber longer than 0.0143 cycle/km. This map performed clearly noises anomalies allover the study area, trending mainly in the E-W and ENE directions.

Band-pass filtered is made by passing wavenumber between 0.0344– 0.0072 cycle/km to construct true anomalies magnetic map (Fig.13). This map seems to be noisier than the original one since it emphasis the short wavelength anomalies. The positive and negative local anomalies, which could propose, fault structures in the form of highlands and lowlands, respectively. The residual magnetic anomalies show three major orientations in ENE, NE, and E-W directions. The northern parts characterized by negative anomalies (between wells no. 3 and 30) that may be related to northern Western Desert basin. The southern and the central parts exhibit sharpness zones of high amplitudes, which may be related to Alamein high (south well no.25) and Ras-Qattara high in southern parts.
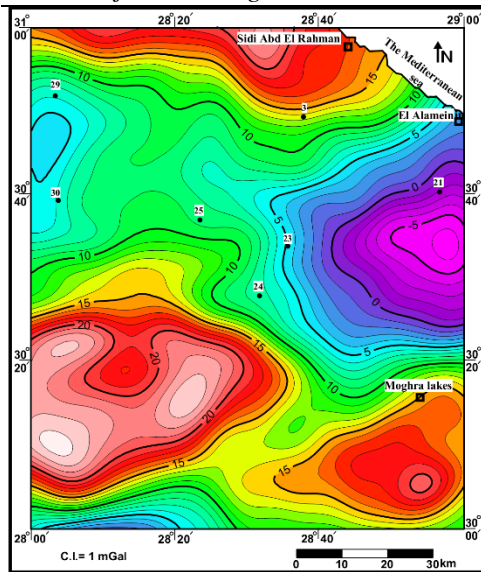
Fig. 8: Low-pass filtered gravitymap with 0.0145 cycle/kmcut-off filter.
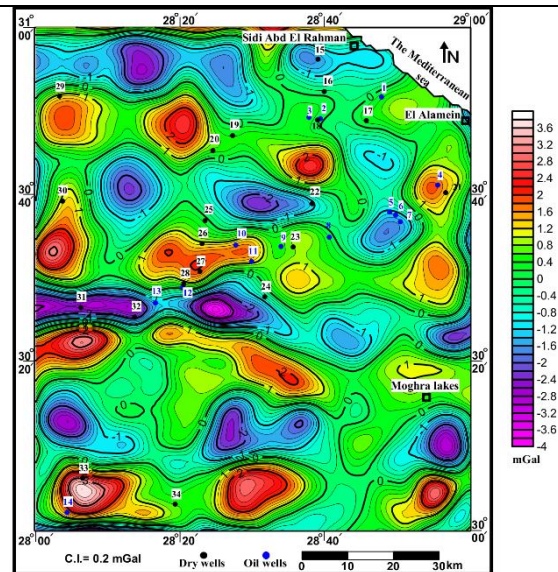

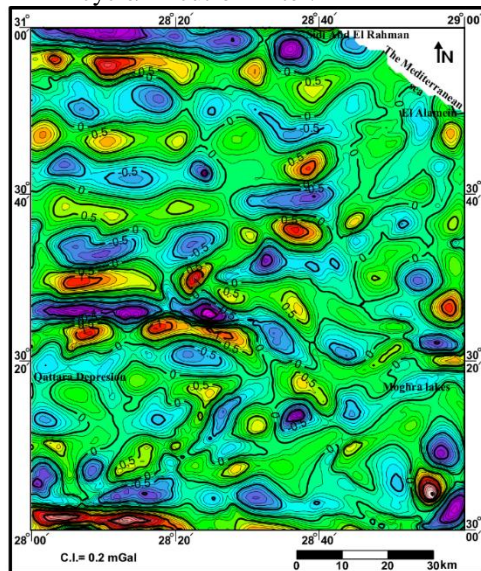Fig. 10: Band-pass filtered gravity map between 0.0277- 0.0073 cycle/km.

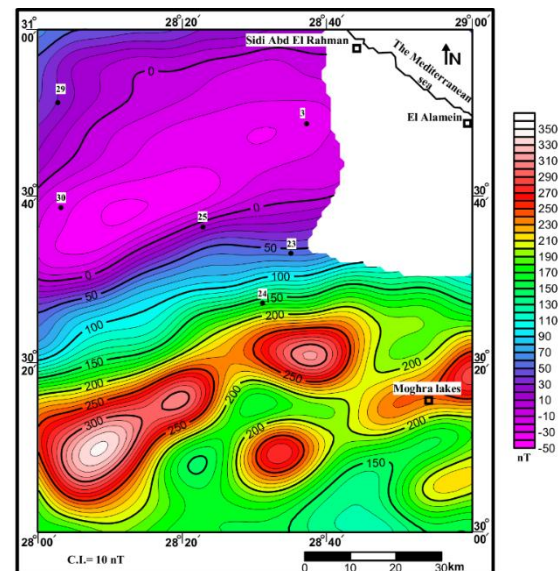Fig. 9: High-pass filtered gravity map with 0.0145 cycle/km cut-off filter.

Fig.11: Low-pass filteredmapwith 0.0173 cycle/km cut-off filter of RTP magnetic map.
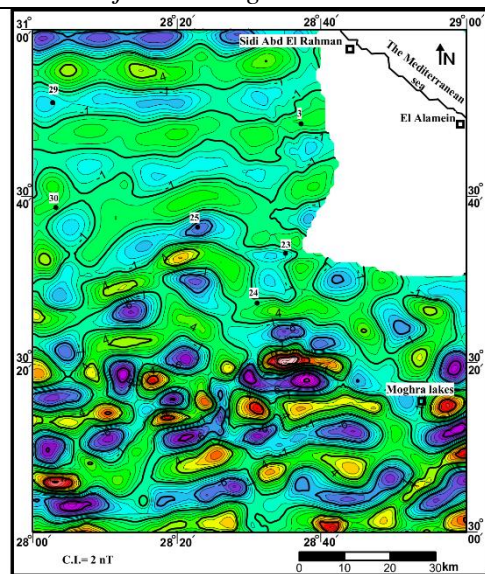
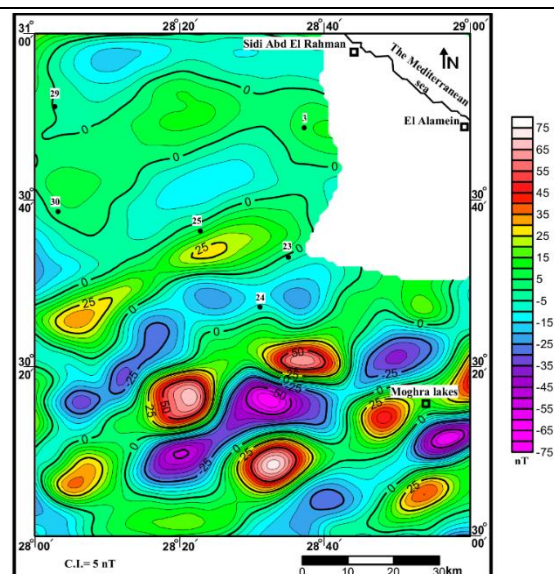Fig.12: High-pass filtered map with 0.0173 cycle/km cut-off filter of RTP magnetic map.

Fig.13: Band-pass filtered mapbetween 0.0344– 0.0072 cycle/km of RTP magnetic map.

5.4. Depth estimation technique

In geophysical investigations of the subsurface structures, the most important parameter to be estimated is the depth to the anomalous structure. For hydrocarbon exploration, this is usually equivalent for determining the maximum thickness of the sedimentary section or the location of igneous intrusive in the section. The magnetic method is extensively used for determining the depth to magnetic crystalline rocks and especially the basement underlying surface sediments and sedimentary rocks, which are essentially transparent to magnetic fields [23]

Spectral analysis technique is applied on the RTP map (Fig.5). In this method, the magnetic profiles in the space domain are transformed into frequency domain using [24] method and the various parameters of anomaly sources are derived from the characteristic properties of the amplitude.

Figures (14. a) and (14. b) illustrate an examples of the spectral analysis technique along the selected profiles of RTP map. Where, the estimated depths results to the basement surface are shown in (Table.3). The depths range from about 3.03 km (M6) to more than 5.92 km (M3) in the eastern part. There is a general increasing in the depth to the basement rocks to the northern part as revealed from profiles M11, M12, M15, M16, M17 and M18. The maximum depth value attains about 7.24 km at the centre of main basin (the northern Western Desert basin). The depths to the intruded bodies also increase from south to north. It ranges from 0.4 to 1.21 km as shown in the (Table.2). Generally, spectral analysis technique gives a satisfied results as compared with available depths recorded from different drilled wells, where some profiles passes through or nearing it, M15, M16, M18, M20, M21 and M22 as shown in (Table.3).
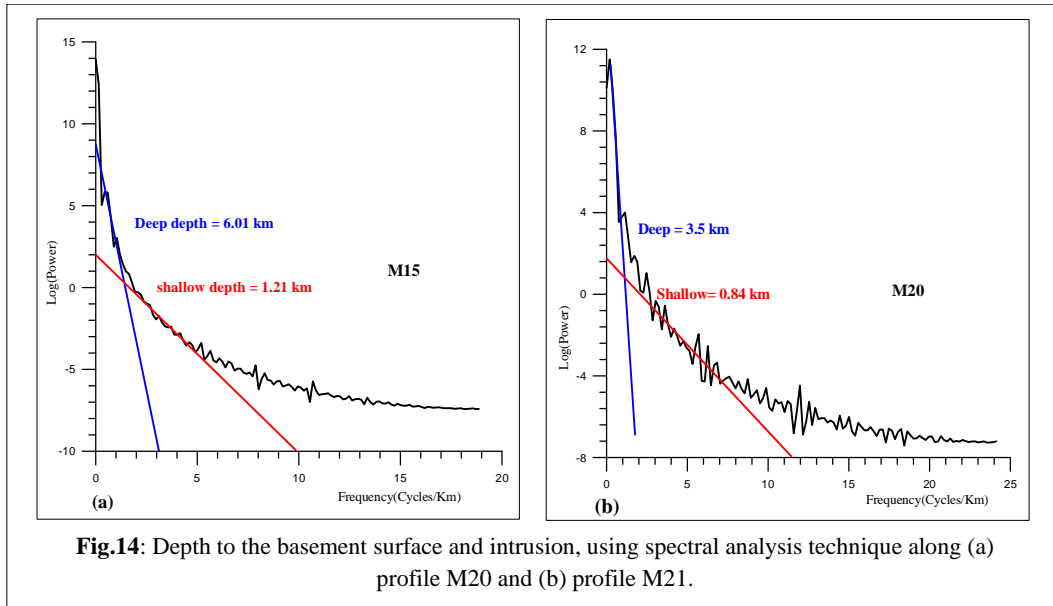
Fig.14: Depth to the basement surface and intrusion, using spectral analysis technique along (a) profile M20 and (b) profile M21.

Table.2: Depth estimation results of RTP magnetic anomalies for spectral analysis methods.

Profile no.	Spectral analysis	
	Basement (km)	**Intrusions (km)**
M1	5.01	0.82
M2	4.78	0.75
M3	5.92	0.67
M4	5.13	0.46
M5	3.97	0.67
M6	3.03	0.45
M7	5.41	0.62
M8	4.68	0.52
M9	3.45	0.64
M10	3.51	0.55
M11	6.48	1.1
M12	6.28	0.84
M13	5.51	0.74
M14	3.27	0.62
M15	6.01	1.21
M16	6.65	1.08
M17	7.24	0.76
M18	6.44	0.73
M19	4.4	0.6
M20	3.5	0.69
M21	4.5	0.67
M22	5.56	0.65
M23	5.86	0.47

Table.3: Comparison between the calculated depths from spectral analysis technique along RTP profiles passes through wells and the recorded depths of these wells.

Profiles	Calculated depth (Km)	Wells	TD(Km)	FMTD
M15	6.01	Ig-34-1	4.57	Khattatba
M16	6.65	ALAMEIN-	4.39	L. Cretaceous
M18	6.44	GANAYEN-	4.86	Khattatba
M20	3.5	S. DABAA	2.9	Basement
M21	4.6	ALMAZ-1	4.1	Basement
M22	5.56	FADDA-1	4.81	Khattatba

5.4. Euler's deconvolution technique

Euler's deconvolution (ED) is commonly used as a second step in the interpretation of magnetic and/or gravity data, wherever the Euler deconvolution is used to correlate the magnetic data with geologic map and to

confirm the modeling results, because it is both a boundary finder and a depth estimator [25]. It uses the magnetic distributions such as point poles or dipoles as a source of the potential field anomalies, these different source types are characterized by a factor known as the structural index (SI).

Euler's deconvolution method is applied on RTP data using standard 3D Euler package, included in the [21] on the basic of [26] theory.

Theory:

The Euler's homogeneity equation relates the field (magnetic or gravity) and its gradient components to the location of the source, with the degree of homogeneity (N), which may be interpreted as structural index (Thompson, 1982).

$$\frac{\partial f}{\partial x}(x - x_0) + \frac{\partial f}{\partial y}(y - y_0) + \frac{\partial f}{\partial z}(z - z_0) = SI(B - T) \qquad (1)$$

Where:

T is the observed field at location (x, y, and z) and B is the base level of the field (regional value at the point (x, y, and z)) and SI is the structural index or degree of homogeneity. The equation is solved for the source position by passes a moving window through the data, and uses least-squares inversion to obtain the depth and horizontal location of sources with different structural indices. Usually the structural index (SI) is fixed and the locations and depths (x_0, y_0 and z_0) of any sources.

Therefore, it requires three orthogonal gradients (two horizontal and vertical gradients) of the magnetic or gravity data, which (if they have not been measured) are normally, calculated using theFFT. The equation is solved for the source positions by passes a moving window through the data, and uses least-squares inversion to obtain the depth and horizontal location of sources with different structural indices. Usually the structural index (SI) is fixed and the locations and depths (x_0, y_0 and z_0) of any sources.

Figure (15) shows the application of ED, using SI=0 and window size=20, which in magnetic field interpretations indicates contact [23]. This map shows the ability to estimate major vertical contacts separates different subsurface magnetic bodies, which are shown in the northern part and trending in the E-W and ENE directions, with different depth from 2 km to more than 6 Km. These solutions locates the limits of Dabaa high. The middle and the southern parts show the source locations that surrounding most of anomalies and parallel to major faults, trending mainly in the ENE to NE and E-W directions. The solutions depths reached to 4 km in almost of the study area and may be extended to 6 km on minor locations, which may be related to the main basins such as Alamein area and its extensions.
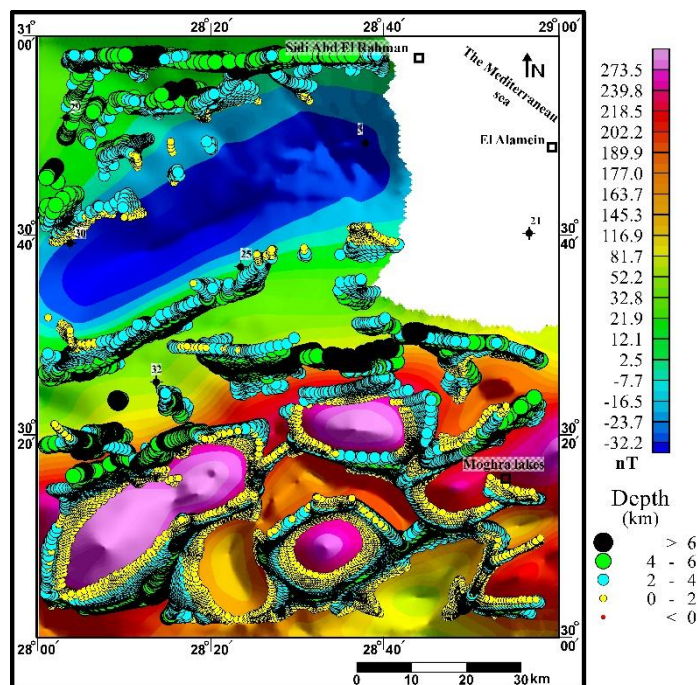

Fig. 15: Contact locations and their depth (0-6 Km), as deduced from the RTP aeromagnetic map, using standard Euler's deconvolution.

5.5. Tilt Angle Derivative (TAD) technique

One important goal in the interpretation of magnetic data is to determine the type and the location of the magnetic source. This method estimates both the horizontal location and the depth of magnetic bodies, but

without specifying prior information about the nature of the sources structural index [27]. [28] showed that the tilt angle value ranges between ±π/2.Zero line is directly over the contact, thus locating the position of anomalies contact.

The TAD technique is applied on RTP aeromagnetic map (Fig.16), using [21] program on the basic of [29] theory.

Theory

The tilt angle derivative (TAD) [29]is defined as

$$TAD \text{ or } \theta = \tan^{-1}\left(\frac{VDR}{THDR}\right) \ldots\ldots(2)$$

Where θ is the local phase, VDR: is the vertical derivative and THDR is the total horizontal derivative.

This map exhibits major uplifted blocks with the main magnetic trends E-W and ENE direction, where TAD is relatively smoother and positive value over the sources. The northern parts show major uplifted trending in E-W direction. In addition, the middle part (south well no. 25) shows high local anomalies, trending NE direction and it can be correlated to Alamein high. In addition the southern part exhibits uplifted area, with NE to ENE and E-W directions, which may be associated to Ras-Qattara high. Large low area appeared in the northern part between well no.3 and 30.

It is interesting to note that the TAD tends to convey the edge detection from uplifts at all scales and depths, also, the distance between zero to π/4 contours is used to estimate the depths to sources. The results of depth estimation ranges from 2.5 to 4.5 km in southern parts. In the same time, the depths attain from 3 to 4 Km in middle parts (south well no. 25), while reached to more than 6 Km in northern parts.

In order to ensure the source edge location, Euler's deconvolution is plotted over the tilt angle derivative map (Fig.17). This map displays a good correlation between Zero lines and ED solutions location allover the investigated area. Where, Euler solutions tend to be clustering along edges of source as contact and/or faults. In addition, the tilt angle derivative determines the edges of uplift blocks as shown in the northern (north well no. 29), the middle (south well no.25), and the southern parts.

In addition, Zero line and ED solutions may help us to delineate edges of major basins as shown in middle (Alamein basin) and northern (The northern Western Desert basin) parts.
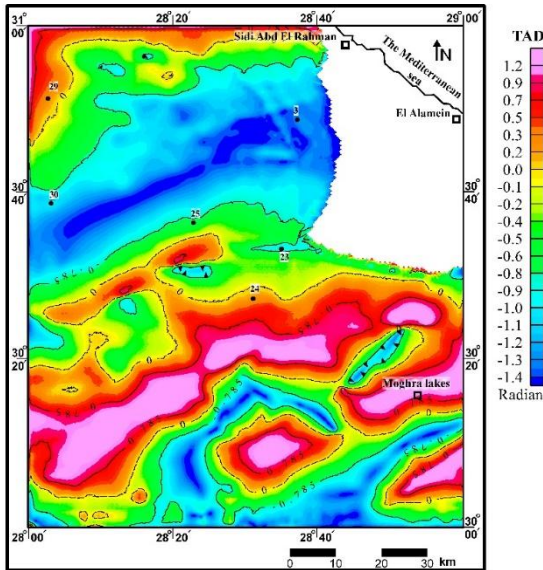

Fig. 16: The TAD of the RTP aeromagnetic map of the study area.
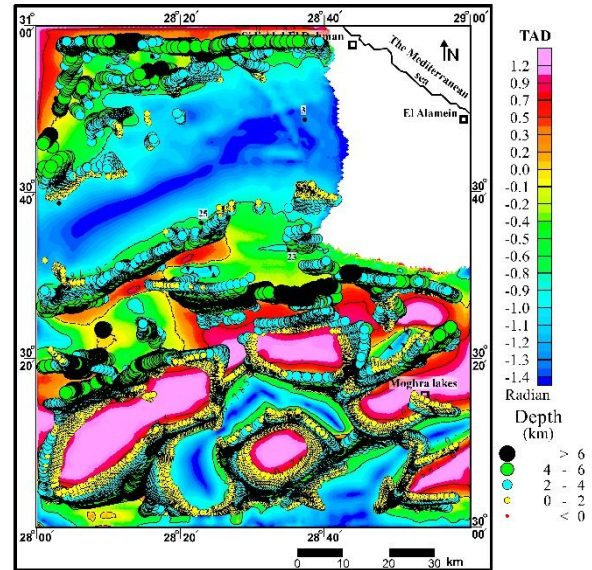

Fig. 17: Euler's deconvolution solution obtained from the RTP aeromagnetic map, plotted over the TAD map.

5.6. Structure tectonic map

Tentative structure basement map (Fig.18) is constructed by delineating the edges of uplifted and downfaulted blocks deduced from separation magnetic maps ([23], [30] and [31]). In addition, the vertical faults separated high and low blocks from each other and strike-slip faults can be predicted from ED solution and TAD aeromagnetic maps.

This map is characterized by the presence of five alternative uplifted and down-faulted blocks, resulted from ENE to NE dip-slip faults. The southern part shows downfaulted blocks namely, L_1, L_2, and L_3 alternative

with uplifted blocks namely; H_1, H_2, and H_3 trending ENE and E-W directions. Thesestructuresareintersected by younger NW to NNW strike-slip faults F_1 and F_2 lead to forming sub-parallel downfaulted and uplifted area. On the other hand, the northern part exhibits H_3 and H_4 uplifted blocks in the same directions, separated by downfaulted area L_5.

In briefly, tentative structure basement map shows several uplifted and downfaulted area, where the northern uplifted block H_4can be associated to Dabaa high. Inaddition, the middle block H_4can be correlated to Gibb-Afia /Alamein high. These uplifted blocks is separated by block L_5, which can be related to the northern Western Desert basin. Furthermore, the southern parts indicated presence of uplifted blocks H_2 that can be related to Ras-Qattara high. While, down faulted blocks L_4 can be considering as the main basin in the study area (Alamein basin).
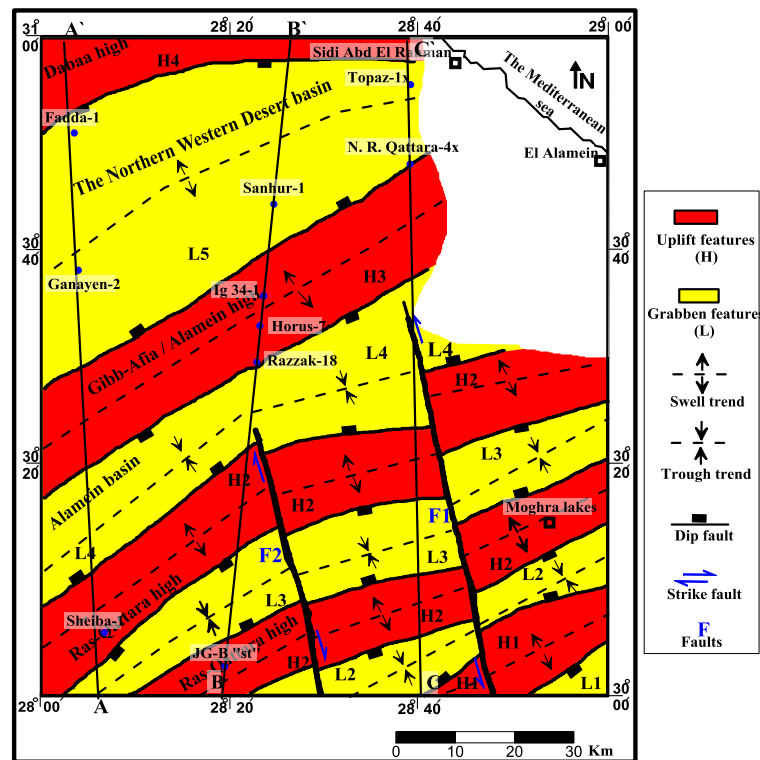

Fig.18: Tentative basement structure map of the study area as deduced from the integration of analytical techniques showing the location of 2.5D modelled profiles.

5.7. 2-D and 2.5-D Modeling technique.

Forward modeling technique is applied on both gravity and magnetic maps, to confirm the tectonic framework in the interested area. In this study, 2-D/2.5-D modeling along three profiles are carried out using [32] program that based on the algorithm of [33] and [34]. These profiles namely from west, A-A`, B-B` and C-C') plotted in the same location on both Bouguer (Fig.4) and RTP magnetic (Fig.5).They run in the south to north direction to reflect the basement surface and tectonic elements take into account the following aspects:

1- First step began with using 2-D gravity modeling profiles to confirm depths to basement surface, Conrad and Moho discontinuities. Spectral analysis technique is applied to the modeled profiles A-A`, B-B` and C-C` for gravity data (Fig.19) to estimate average depths to these boundaries (Table.4). This step has two benefits. Firstly, to eliminate errors caused by survey line that may be not oriented perpendicular to the strike. Secondly, there is no dependence on user-selected window size, which other techniques require, which in most cases is easier to approximate with a straight line and denoting deeper discontinuities (Moho and/or Conrad) [35].

2- The results of depth estimation along three profiles of magnetic data (Fig. 20) are used to determine the depths to Curie isotherm and basement surface (Table.5). The estimated average depths are shownin tables (4) and (5). Theyshowcomparable results with the depths to basement, Conrad and Moho discontinuities that carried out bydifferentauthors on crustal modeling ([31], [36], [37], [38], [39] and [40]).
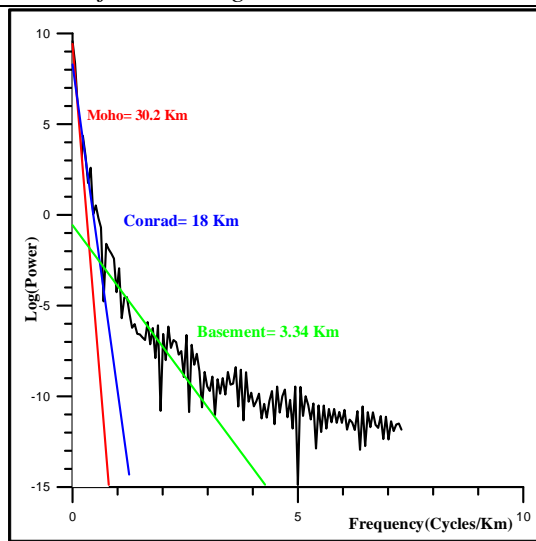
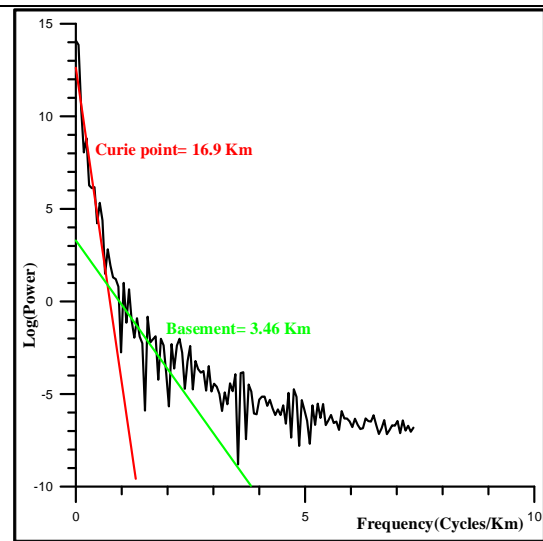Fig.19: Spectral analysis results along gravity profile A-A`.

Fig.20: Spectral analysis results along magnetic profile A-A`.

3-The distance between basement and Curie surfaces is divided into many blocks based on structure criteria, which were deduced from tentative basement tectonic map (Fig.20).

4- These profiles passes through different wells, so the sedimentary cover may be divided into number of layer according to available data from drilled wells reached to different formations as shown on (Table.1).

5- The densities vary for both sedimentary layers and crustal layers according to many parameter. The assumed densities of the crustal models of the study area show a good and satisfied results as compared with rock densities values used in several studies for the adjacent areas ([31], [37], [38], [40], [41], [42], [43], [44], [45], [46] and [47]) (Table.6).

Table.4: Results of spectral analysis along the Bouguer gravity profiles modeling

Gravity modeled profiles	Depth of Moho (Km)	Depth of Conrad (Km)	Basement depth (Km)
A-A`	30.2	18	3.34
B-B`	34	-	4.1
C-C`	31	17	3.9
Average	31.7	17.5	3.78

Table. 5: Results of spectral analysis along the RTP aeromagnetic profiles modeling

Magnetic modeled profiles	Curie isotherm depth (Km)	Basement depth (Km)
A-A`	16.9	3.46
B-B`	15.6	4.9
C-C`	18	5.2
Average	16.8	4.52

The first profile A-A` (Fig.21) passes through three wells, where Sheiba-1 well (Paleozoic rocks are recorded at depth of about 2.5 Km), while Mesozoic rocks recorded in wells Ganayen-2 and Fadda-1 at depths of 4.86 Km and 4.8 Km, respectively. The second profile B-B` (Fig.22) lies in the central part of the investigated area. This profiles runs through five wells (JG-B, Razzak-18, Horus-7, Ig 34-1 and Sanhur-1 wells) with different recorded formation (Table.1). Two drilled wells reached to the Paleozoic and Mesozoic are located along third profile C-C` (Fig.23), namely N.R.Qattara-4X and Topaz-1X wells, at a depth attain about 2.4 Km and 3 Km, respectively.

All profiles show that the lower crust- upper mantle boundary (Moho discontinuity) is slightly shallower to the north direction. The thickness of the crust (depth to Moho) ranges between 31.5 km at the southern part and decreases to reach about 28.5 km at the extreme northern rim. The depth to Conrad discontinuity varies from 22.3 km at the southern part to 17.6 km at the northern part. Furthermore, the mean density assumed to be 2.7 g/cc for the Precambrian igneous, 2.9 g/cc for the lower crustal layer (mafic rocks), while upper most part of the mantle is 3 g/cc.

Table.6: Density correlation chart from different studies.

Layer Name	Sedimentary	Upper Crust	Lower Crust	Mantle
Jacobs, (1959)	-	2.67	3	3.3
Makris, (1976)	-	2.82	2.9	3.34
Ginzburg, (1987)	2.5	2.8	2.96	3.25
Setto, (1991)	2.6	2.68	2.9	3
Omran, (1998)	2.3	2.67	3	3.3
Ismail, (1998)	2.4	2.7	3.1	3.47
Omran, (2001)	2.37	2.67	3.07	3.44
Salem, et al, (2004)	2.1(Upper) 2.5(Lower)	2.7	2.93	3.3
El-Khadragy, (2010)	2.43	2.74	2.93	3.28
Saada, et al, (2013)	2.1(Upper) 2.5(Lower)	2.7	2.93	3.3
Azab, (2014)	2.41	2.75	2.9	3.31
Present Study	(2.19)Cenozoic (2.37) Mesozoic (2.45)Paleozoic	2.7	2.9	3

Figures (24, 25 and 26) exhibit magnified picture for magnetic portion along A-A', B-B` and C-C` modeled profiles, respectively. The upper part of model shows sedimentary covers, which divided into three modeled layers Paleozoic, Mesozoic, and Cenozoic according to the obtained depths from the drilled wells. Paleozoic rocks are characteristic by high-density value = 2.45 g/cc; Mesozoic rocks have a medium density value = 2.37 g/cc and upper Cenozoic portion with a minimum density = 2.19 g/cc along A-A` and B-B` modeled profiles. The densities values are assumed and correlated with different values obtained from previous works of surrounding areas ([31], [40], [47],).

The estimation depths results to basement surface along three profiles are shown in (Table.7). These results show good agreement between these profiles, which supported our assumption to build up the magnetic layer according to structure criteria. Figures (24, 25 and 26) show 2.5-D blocks, these blocks extend from basements surface to Curie point surface (depth= 17 km). These figures display two main basins in middle part Alamein (L_4) and the northern Western Desert basins (L_5) blocks, furthermore, three uplifted region show in southern, middle and northernmost parts. The southern uplifted block H_2, which may be associated to Ras-Qattara high, while, the middle uplifted block H_3 is related to Alamein high. Finally, block H_4 in northern part can be related to Dabaa high. Paleozoic and Mesozoic layers tend to be thinning over the horst block area in southern and northernmost parts as compared to the very thick section on the downthrown side of the two main basin

In addition, Magnetic portion along these profiles show some similarity. The rock susceptibilities show gradual increase toward the southern part, where, the magnetic susceptibilities along this trend vary greatly from 0.001 (H_4) to 0.0098 (L_3) cgs-units. Furthermore, the density values show slight increase toward the southern and northern parts from middle part.
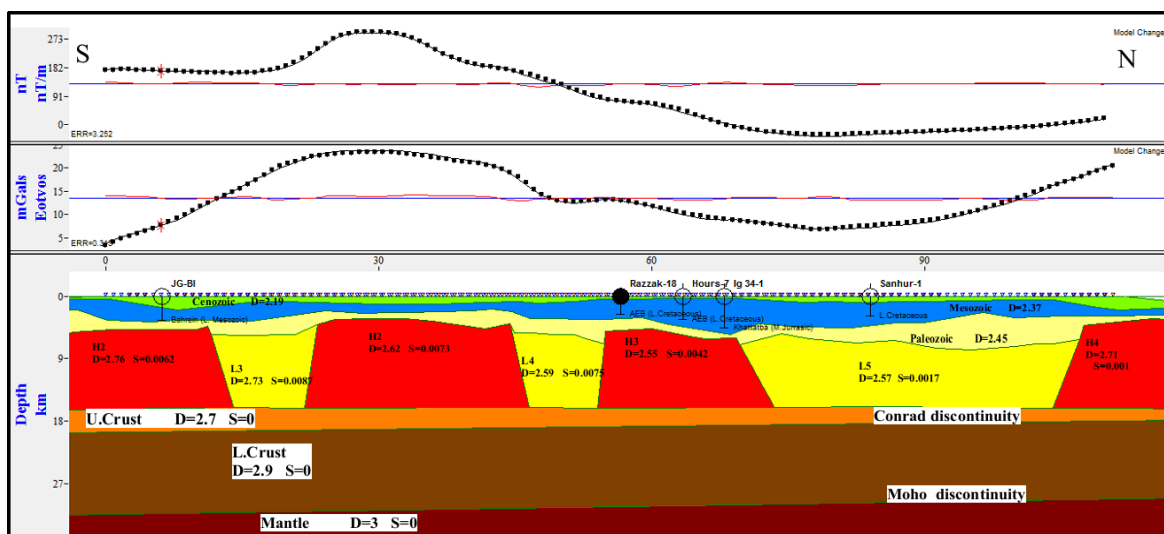

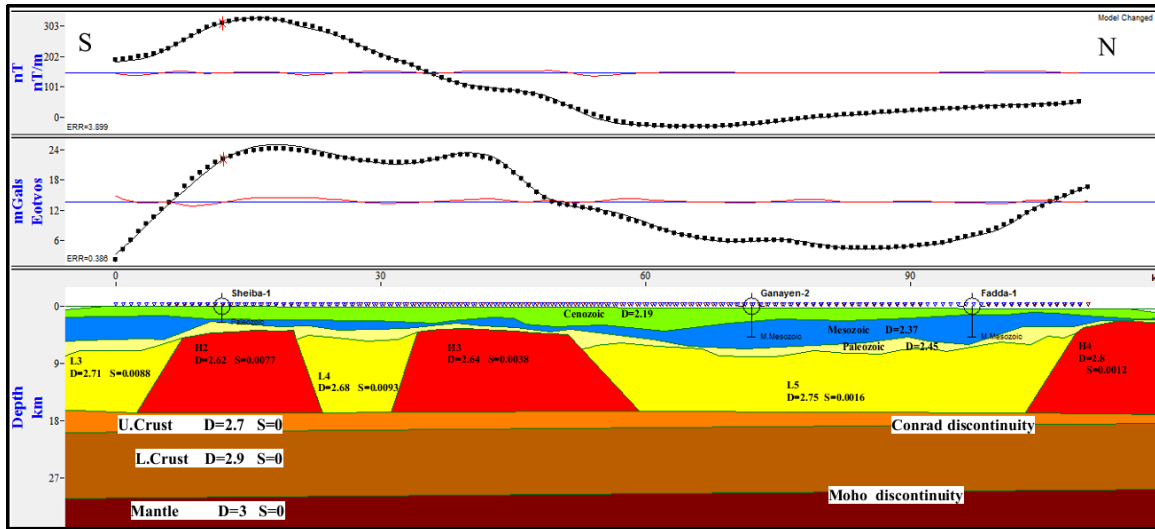Fig.21: Crustal modeling along profile A-A`.

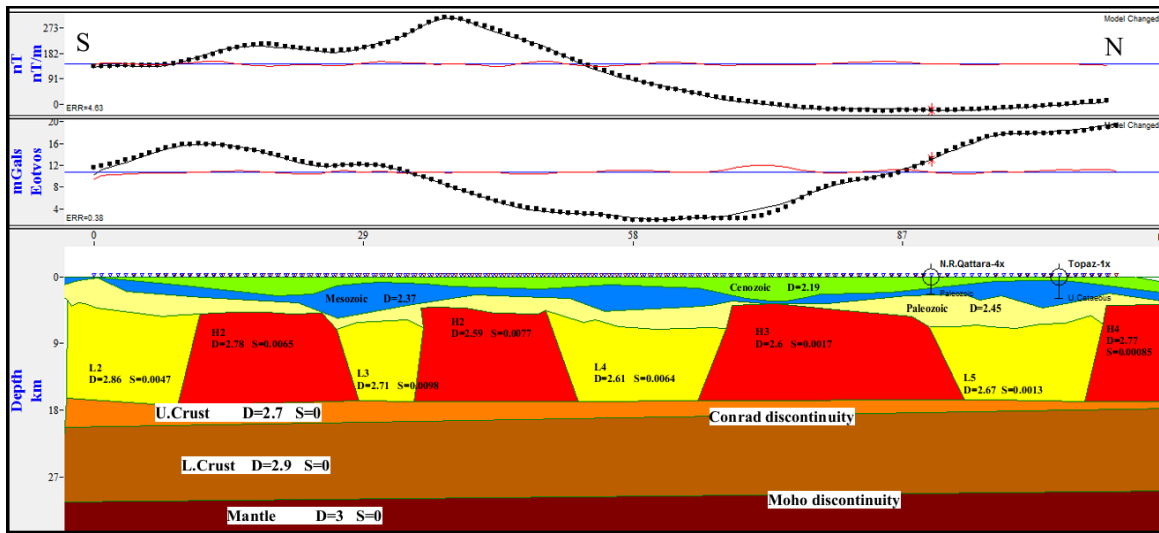Fig.22: Crustal modeling along profile B-B`.

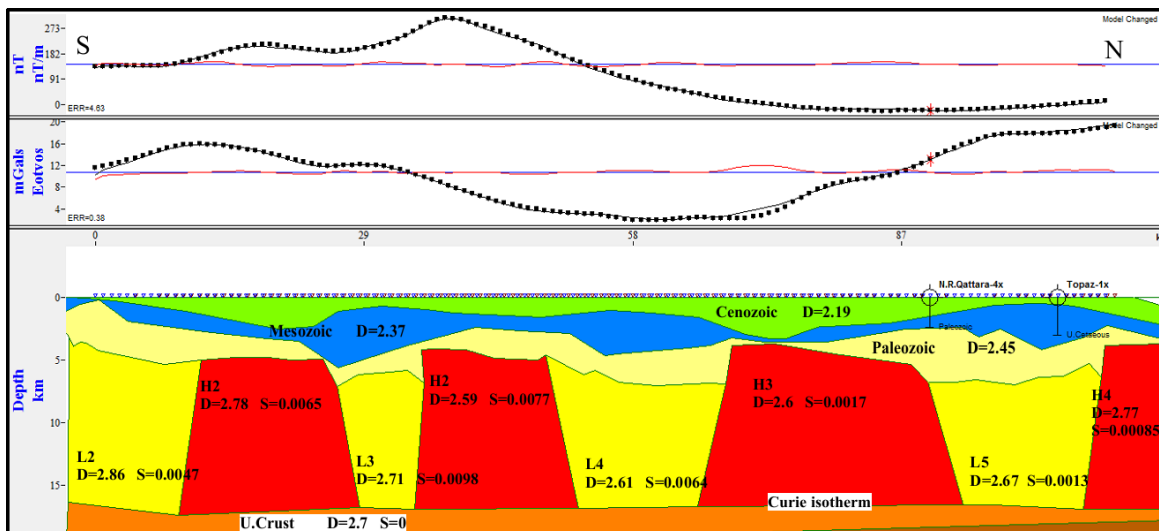Fig.23: Crustal modeling along profile C-C`.

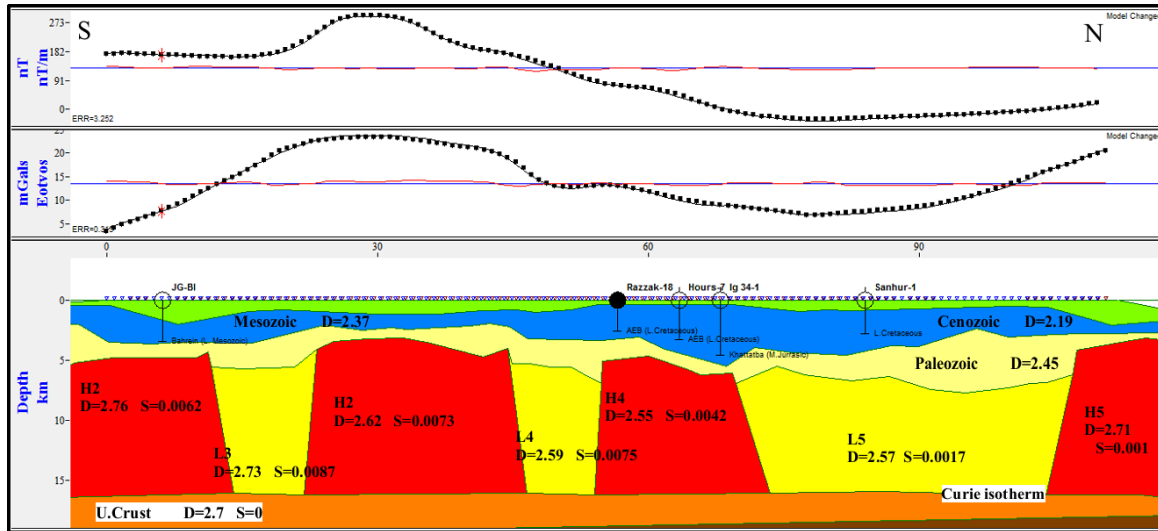Fig.24: Magnified picture of magnetic portion along profile A-A`.

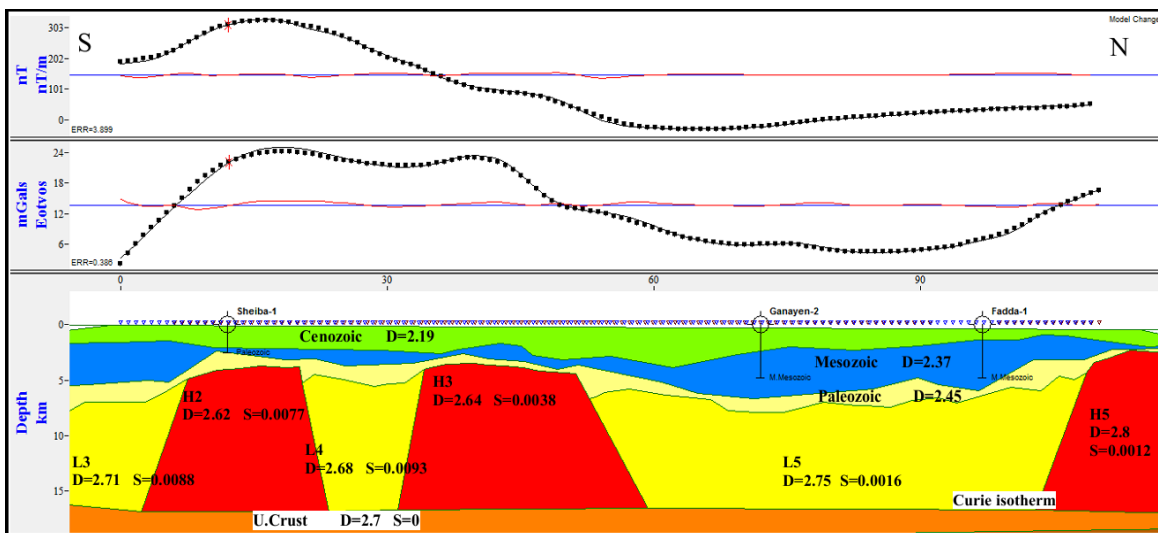Fig.25: Magnified picture of magnetic portion along profile B-B`.

Fig.26: Magnified picture of magnetic portion along profile C-C.

Table.7: Depth estimation to basement surface from three modeled profiles.

Blocks	A-A` (depth to basement) (km)	B-B` (depth to basement) (km)	C-C` (depth to basement) (km)
L3	6.8	5.6	6
H2	3.6 – 4	3 – 4.8	4 – 4.5
L4	5.5	6.8	6.9
H3	3.3 – 4	4.7	3.8
L5	7	7.7	6.9
H4	3	3.8	3.6

5.8. Tentative basement relief map

The average depth results from the applications of different spectral analysis methods, and the 2.5-D modeling as well as depths from the available drilled wells are used to construct a tentative basement map of the study area (Fig.27). It shows that the depth to the basement rocks ranges from 2.3 km to more than 7.6 km. In the southern part, the depth to the basement rocks varies from about 3.5 to 4 km, revealing uplifted area. While, the middle parts display two different area, Alamein high and Alamein basin, with depth values of 2.5-4.3 and 5-6.5 km respectively. In addition, the depth to the basement rocks varies from about 3.5 km (Dabaa high) to more than 7.5 km inside the northern Western Desert basin.
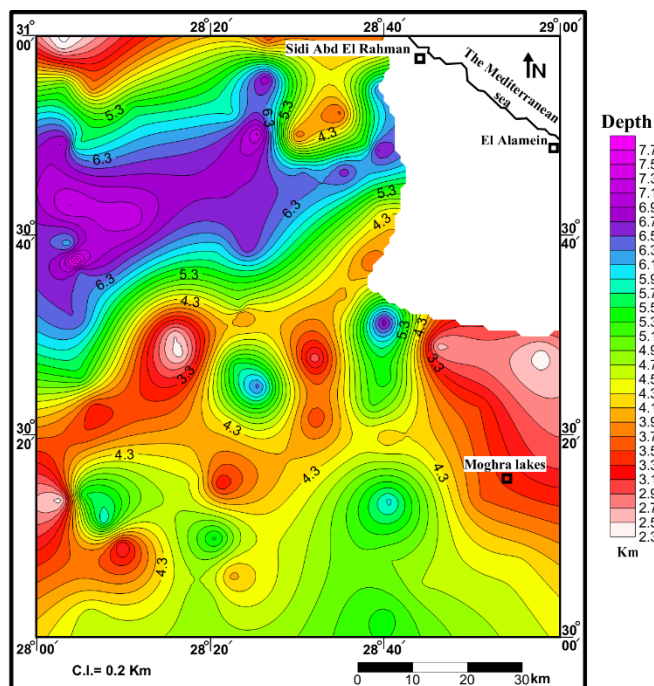
Fig.27: Basement relief map of the study area.

VI. Discussion and Conclusions

The potential field data of Alamein area had been analyzed and integrated with other geophysical and geological studies to extract deep subsurface structures and depth to buried basement rocks. Different authors (e.g. [1],[2], [48], and[49]) constructed subsurface structure maps in Western Desert according to potential data, seismic and well logging interpretation, there are some differences between subsurface structure on these maps, which may be related to use old techniques and/or type of the used data. Therefore, the present study is interested in delineating deep basement structure locations, extensions, trends, and depths then correlated them with modeling technique to support our results.

Generally, analysis of high gravity values in southern and northern parts may be due to (i) thinning of the earth's crust towards the coastal zones, or (ii) the presence of intrusive bodies with higher density than the country rock, or (iii) the presence of more dense or shallow subsurface rocks ([35]). Deep seismic studies and gravity modeling by [36] revealed a flat Moho with slight thinning towards the Mediterranean Sea coast, which decay second assumption. Furthermore, the northern Western Desert especially Alamein area didn't contain any information or studies proved presence of intruded bodies into sedimentary covers. One of the possibilities may be a shallow and/or high-density body. Therefore, the combined gravity and magnetic models highlight this aspect and support the last assumption.

The results of band-pass filtering display that the southern positive gravity anomalies lie in the same location of the positive magnetic ones revealing uplifted structures, this interpretation becomes acceptable because the structure is upheaval, which means that the basement rocks have been brought closer to the surface. However, the northern rim displays positive gravity, which may be related to transition zone, but when correlating it with magnetic data shows strong positive anomaly. This correlation supports the presence of uplifted high in northernmost part. On other hand, other portion of the study area in the eastern and middle parts is almost associated with negative gravity and magnetic anomalies. This is also realistic since these parts are almost filled with a thick column of non-magnetized sediments, where depth reached to 7.24 km (east well no. 30). The tilt angle derivative tends to be maximum over source bodies, while the edges of anomalies coincident with zero contour lines. Therefore, correlation between Euler's deconvolution solution and TAD techniques, which is applied on RTP aeromagnetic map, exhibits a good relation between ED solutions and zero contour lines, coincident with contact or faults of basement structure. This correlation side by side with FFT filtering helps us to constructed more reliable structure map.

The results of tectonic map achieved by this study were correlated to the previous studies to indicate the similarity and the difference between these results according to their subsurface structure features as locations, extension, and trend. The present map displays three uplifted blocks namely, Ras-Qattara in southern part with NE to ENE and E-W trends, Alamein high in middle part trends NE direction and Dabaa high in northernmost part with an E-W direction. While, the main basin (Alamein basin) lies in the middle part between Ras-Qattara and Alamein, as well as the northern Western Desert bounded in northern part by two uplifted

Alamein and Dabaa highs. These results is more appropriate with subsurface structure location interpreted by [1], where basement mega structure map shows one uplifted namely, Shieba (Ras-Qattara) high lie in southern part of the study, trending mainly in the E-W direction. Also, the results are more appropriate with Structure maps constructed by [2] and [49], where the preset map shows new uplifted in northern rim (Dabaa high). In addition, the present study shows Ras-Qattara high with NE to ENE trends directions, which disagreement with previous study, but [3], suggested that the Sheiba high basement blocks trending NE direction formed during the Early Jurassic and were not significantly affected by subsequent tectonic events.

The modeling process depended on various parameter to minimizing errors, where building 2-D gravity modeling according to the average depth results to discontinuities surface, which extracted from power spectrum curves and assuming densities. However, 2.5-D magnetic modeling was carried out according to the calculation of average depths to the curie isotherm (17 km) and structure features obtained from basement structure map. The modeled profiles reveal high southern anomalies linked with uplifted blocks (H_2) (3 − 4.8 km depth) of relatively high density and susceptibility. While, the middle part comprises two downfaulted blocks (L_4 and L_5), with depth range from 5.5 to 7.7 km, where blocks (H_3) separates the previous basins. Finally, the northern rim show strong uplifted area (H_4) with depths ranges between 3 and 3.8 km. In addition, increase densities from middle to southern and northern parts with shallow depths supported our assumption about southern and northern anomalies and made the present structure map more logically from previous studies.

The basement relief map of the investigated area clearly indicates that, the depth to basement surface is a little difference between the results comes from basement map constructed by El, Paso co., (2011). The basementdepth of the study area varies from 2.7-3.6 km in southern and northernmost parts and increase to 4.8-6.5 km in the other parts. Shallow area appears in middle part with depths range from 2.5-4.3 km, which may be associated to Alamein high.

Acknowledgements

Reference

[1]   G. Hantar. North Western Desert. In R. Said, ed., The Geology of Egypt. (Rotterdam, Netherlands, A. A. Balkema Publishers, 1990), 293-319.
[2]   W.M. Meshref. Well evaluation conference of Egypt. Schlumberger Technical Editing Services, EGPC, Egypt, 1995, 87 p.
[3]   A.W. Wescot,A. Mahmoud, C.B. David, M.C. Roger, T.G. Steven, A.M. David, W.H. Walter, D.W. Amanda, C.D. John and S. Adel. Jurassic Rift Architecture in the Northeastern Western Desert, Egypt. Adapted from poster presentation at AAPG International Conference and Exhibition, Milan, Italy, October 23-26, 2011.
[4]   C. Fichler, E. Rundhovde, O. Olesen, B.M. Sæther, H. Rueslatten, E. Lundin and A.G. Dore.Regional tectonic interpretation of image enhanced gravity and magnetic data covering the mid-Norwegian shelf and adjacent mainland. Tectonophysics 306, 1990, 183–197.
[5]   S.D. Khan, M.S. Fathy andA. Maha. Remote sensing and geophysical investigations of Moghra Lake in the Qattara Depression, Western Desert, Egypt. Journal. Geomorphology, 207, 2011, 10–22.
[6]   O.A. El Shaarawy. Structural analysis and oil potentialities of the area north of the Qattara Depression, Western Desert, Egypt, based on geophysical and subsurface geological data. Geology Department, Ain Shams University, Cairo. 1994, 196 p.
[7]   MG. Barakat. General review of the petroliferous provinces of Egypt with special emphasis on their geologic setting and oil potentialities: Petro l. And Gas Proj., Cairo Univ., M.I.T., Technology planning program, 1984, 86 p.
[8]   R. Said. The Geology of Egypt. (Elsevier Publ. Co., Amsterdam. Oxford and New York, 1990), 377 p.
[9]   Egyptian General Petroleum Corporation (EGPC). Well evaluation conference of Egypt. Schlumberger Technical Editing Services, EGPC, Egypt, 1984, 64 p.
[10]   R. Said. The geology of Egypt. (Rotterdam, Netherlands, A.A. Balkema Publishers, 1990) 9-734.
[11]   W.M. Meshref. Tectonic framework. In R. Said (editor): The geology of Egypt (Rotterdam, Netherlands, A. A Balkema Publishers, 1990) 113-130.
[12]   Bader Petroleum Company (BAPETCO). Generalized Litho-Stratigraphic Column of Western Desert. Internal report. 2007, 10 p.
[13]   N. Sultan, N. and A. Halim. Tectonic Framework of northern Western Desert, Egypt and its effect on hydrocarbon accumulations. EGPC 9th Exploration Conference, Cairo, Egypt, 1988.
[14]   J.C. Dolson, M.V. Shann, S. Matbouly, C. Harwood, R. Rashed, and H. Hammouda. The Petroleum Potential of Egypt, in W. A. Morgan, ed., Petroleum Provinces of the 21st Century, V. Memoir 74: Tulsa, Oklahoma, American Association of Petroleum Geologists, 2001, 453-482.
[15]   M.I. Youssef. Structural pattern of Egypt and its interrelation. American. Assoce. Petrol. Geol. Bull. 52(4), 1968, 601 - 614.
[16]   R.S. Dietz, andJ.C. Hoden. Reconstraction of Pangea, break-up and dispersion of continents, Permian to present. Journal. Geophys. Res. 75, 1970, 4939-4955.
[17]   W.M. Meshrefand M.M. El Sheikh. Magnetic tectonic trend analysis in northern Egypt. Egypt. Journal. Geol, 17, 1973, 179-184.
[18]   General Petroleum Company. GPC. Bouguer gravity map of Egypt, 1978.
[19]   GUPCO. A high sensitivity aeromagnetic survey of Egypt, 1981.
[20]   S. Raid. Shear zones in the north Egypt, interpreted from gravity data. Geophysics, 42(6), 1977, 1207-1214.
[21]   Geosoft Oasis Montaj Inc. Program of potential field data. Geosoft Inc. Toronto Canada, 2007.
[22]   S.D. Parasnis. Mining Geophys. Method in geochemistry and geophysics (Elsevier Publishing Comp., Amsterdam, London, New York, 1966).
[23]   W.J. Hinze, R.B.V. Ralph and A.H. Saad.Gravity and Magnetic Exploration (Cambridge. England, Camb. Univ. Press, 2013) 512 p

[24]   A. Spectorand F.S. Grant. Statistical models for interpreting aeromagnetic data. Geophys. 35, 1970, 293-302.
[25]   A.B. Reid, D. FitzGerald, and P. McInern. Euler deconvolution of gravity data. SEG Annual. Meeting, Dallas, accepted for presentation, 2003.
[26]   D.T. Thompson. A new technique for making a computer assisted depth estimates from magnetic data. Geophys, 47(1), 1982, 31-37.
[27]   A. Salem, S. Williams, D. Fairhead, R. Smith, and D. Ravat. Interpretation of magnetic data using tilt-angle derivatives. Geophysics, 73, 2008, L1–L10.
[28]   A. Salem, S. Williams, D. Fairhead, D. Ravat, and R. Smith. Tilt-depth method: A simple depth estimation method using first-order magnetic derivatives. The Leading Edge, 26, 2007, 1502–l505.
[29]   B. Verduzco, J.D. Fairhead, C.M. Green, and C. MacKenzie. New insights into magnetic derivatives for structural mapping. The Leading Edge, 23, 2004, 116–119.
[30]   G. Parker. Mapping Geologic Structure of Basement and Role of Basement in Hydrocarbon Entrapment. *Adapted for online presentation from two articles by the author in AAPG Explorer (November and December, 1999), respectively entitled "Basement Mapping Highly Crucial" and Maps: It's the Basement's Fault. Search and Discovery Article #40052.
[31]   S.A. Saada, H. Zahra, and A.A El-Khadragy. Structural Pattern and Crustal Modeling of the Central Northern Part of Egypt, Using Bouguer Gravity Data. Journal. Applied sciences research. 9(10), 2013, 6373-6386.
[32]   Geosoft Oasis Montaj Inc. GM-SYS modeling program of potential field data. Geosoft Inc. Toronto Canada, 2007.
[33]   M. Talwani, J.L. Worzel, and M. Landisman, Rapid gravity computation for two-dimensional bodies with application to the Mendocina submarine fracture zone. Journal of Geophysical Research, 64, 1959, 49 – 59.
[34]   M. Talwani, M. and J.R. Heirtzler. Computation of magnetic anomalies caused by two - dimensional structures of arbitrary shape, computers in the mineral industries, part 1, Standard Univ., publications, Geological Science, 9, 1964, 464 – 480.
[35]   El Sayed Selim and Essam Aboud. Determination of sedimentary cover and structural trends in the Central Sinai area using gravity and magnetic data analysis. Journal. Asian Earth Sciences 43, 2012, 193–206.
[36]   J.B. Makris, R.V. Stofen, A. Allam, M. Maamoun and W. Shatta. Deep seismic sounding in Egypt .Part I, the Mediterranean Sea between Crete-Sidi-Barani and the coastal area of Egypt. Part II crustal and upper mantle of the Red Sea coast (UN published), 1979.
[37]   L.A. Setto. A crustal model for the Nile Delta, Egypt, Journal. Geology. 34(1-2), 1991, 279-292.
[38]   A.A. El-Khadragy, M.H. Saad and A. Azab. Crustal Modeling of South Sitra Area, North Western Desert, Egypt Using Bouguer Gravity Data. Journal of Applied Sciences Research, 6(1), 2010, 22-37.
[39]   A.S. Abu El-Ata, S.S. Azzam, A.A. El- Khafeef, H.S.Zahra and H.T. Oweis. Contribution of Potential Field Data in Delineating the Structural-Tectonic Set-Up ofthe Eastern Qattara Depression Area, Western Desert, Egypt. Aust. Journal. Basic and Applied Sciences, 6(3), 2012, 204-223.
[40]   A.A. Azab. Agnes high, Western Desert, Egypt: A structural study in view of potential data modeling. Egyptian Journal of Petroleum, 23, 2014, 229–245.
[41]   J.A. Jacobs, R.D. Russalland W.J. Tuzo. Physics and Geology .McGraw-Hill, Tronto, 1959.
[42]   J. Makris. A dynamic   model of the Hellenic Arc deduced from   geophysical data. Tectonophysics, 36, 1976, 339-346.
[43]   A. Ginzburg and Z. Ben Avraham The deep structure of the central and southern Levant continental margin. Annual.Tectonicae, 1, 1987, 105-115.
[44]   M.A. Omran and H Fathy. Structural evolution of the Nile cone area. Egypt. Journal. Geology, 42(1), 1998, 273-291.
[45]   M.A. Ismail. Geophysical studies in northern part of Egypt. Ph.D. Thesis, Cairo University. 1998, 96 p.
[46]   M.A. Omran. Crustal modeling of central Nile Delta region. Annual. Geology. Survey, 2001.
[47]   S.R. Salem, S.O. El-Khateeband M.F. Mousa. Structure and evolution of North African passive margin crust: As inferred from 2-D gravity modeling of Nile Delta and its surrounding areas, Egypt. Egyptian Geophysical Society Journal. 2(1), 2004, 17-29.
[48]   T. Bayoumi. In The influence of interaction of depositional environment and synsedimentary tectonics on the development of some Late Cretaceous source rocks, Abu Gharadig basin, Western Desert, Egypt. Paper presented at the 13th Petroleum Exploration and Production Conference, Egyptian General Petroleum Corporation, Cairo. 2, 1996, 475-496.
[49]   Z. El Sisi, M. Hassouba, M.J. Oldani, and J.C. Dolson, The geology of the Bahariya Oasis in the Western Desert of Egypt and its archeological heritage: AAPG Search and Discovery,2001. Article #10032.